Biochar granulation and particle size influence hydrological performance of green roof substrates

Wenxi Liao[1,2] *, Jennifer A. P. Drake[3], Sean C. Thomas[1]

[1]Institute of Forestry and Conservation, University of Toronto, 33 Willcocks St., Toronto, ON, M5S 3B3, ON, Canada

[2]School of Environmental Sciences, University of Guelph, 50 Stone Road East, Guelph, N1G 2W1, ON, Canada

[3]Department of Civil and Environmental Engineering, Carleton University, 1125 Colonel By Drive, Ottawa, ON, K1S 5B6, Canada

* Corresponding author: Wenxi Liao

E-mail address: wenxi.liao@uoguelph.ca

Abstract

Green roofs are increasingly being implemented in cities to improve stormwater management and provide additional ecosystem services. Biochar, a carbon-rich material derived from pyrolyzed biomass, has emerged as a promising substrate additive to improve hydrological performance of green roofs; however, unprocessed biochar is susceptible to erosion loss. Biochar granulation and particle size modification have been suggested as effective approaches to mitigate erosion losses but research on the effects of biochar post-processing on green roof substrate properties and hydrological performance remains scarce. We investigated how biochar granulation and particle size influences surface and pore characteristics and hydraulic properties of green roof substrates. Granulated biochars exhibited uniform surface morphology and pore structure, resulting in consistent hydrological responses across particle size ranges, likely due to the homogeneous structure formed during granulation. In contrast, unprocessed biochars showed a significant increase in Brunauer–Emmett–Teller (BET) specific surface area and pore volume with decreasing particle size. The amendment of granulated biochars improved substrate field capacity, indicating enhanced stormwater retention. In contrast, the addition of fine (0.5–1 mm) and intermediate-sized (2–2.8 mm) unprocessed biochars increased plant available water, potentially enhancing plant performance. Although reduced saturated hydraulic conductivity associated with fine unprocessed biochars may improve green roof detention capacity, fine biochar particle size is expected to increase erosion losses and periodic waterlogging. We conclude that the application of either granulated biochar or intermediate-sized unprocessed biochar provide a balanced enhancement of stormwater retention and detention capacities, as well as improved plant available water in green roof systems.

Keywords: biochar post-processing, surface and pore characteristics, soil water characteristic curve, hydraulic properties, stormwater management, green infrastructure

1. Introduction

Rapid urbanization has led to a proliferation of impervious surfaces in cities, increasing the risks of urban flooding (Chen et al., 2015; Rentschler, 2023). Such flooding can have profound adverse socioeconomic and environmental impacts, including damage to property and infrastructure, contamination of water resources, and loss of life (Hammond et al., 2015). Climate change is predicted to amplify the frequency and intensity of extreme precipitation globally (Madsen et al., 2014; Donat et al., 2016), further exacerbating the hazards associated with urban flooding. It is projected that nearly two-thirds of global population will live in urban areas by 2050 (Ritchie & Roser, 2022), which will pose severe stresses on urban drainage systems and increase the risks of system failure, particularly during extreme precipitation events (Yazdanfar & Sharma, 2015).

Green roofs, which are rooftops with vegetation planted in engineered growing media, have been increasingly implemented in cities to improve stormwater management (Zheng, 2021; Alim et al., 2022). In general, green roofs can mitigate flood risks by attenuating total discharge volume and reducing and delaying peak flows (Li & Babcock, 2014; Palermo et al., 2019). Substrate and vegetation play important roles in hydrological performance on green roofs. Permeable substrates with large pore sizes often show low water retention and detention capacities (Stovin et al., 2015). Vegetation generally enhances green roof water retention and reduces discharge water volume through evapotranspiration (Stovin et al., 2015), water uptake (Wolf & Lundholm, 2008; Nagase & Dunnett, 2012), and rainwater interception by plant aboveground structures (Tan & Wang, 2023). However, green roofs are highly exposed to intense storms, severe and periodic drought, and high wind (Oberndorfer et al., 2007), presenting challenging conditions for substrate and vegetation performance. For example, substrates are

susceptible to particle loss through water and wind erosion (Liao et al., 2022), potentially reducing hydrological performance. In addition, difficult plant growth conditions may result in vegetation degradation, reducing stormwater and ecological benefits of green roof systems. With the intensification of extreme precipitation events under climate change, enhancing hydrological performance of substrates and vegetation is essential for improving stormwater management of green roofs and alleviating pressure on urban stormwater infrastructure (Kourtis & Tsihrintzis, 2021).

Hydraulic conductivity (K) and the soil-water characteristic curve (SWCC) are two hydrological properties of substrates that are fundamental determinants of stormwater retention and plant performance on green roofs. K determines the rate at which water flows through the substrate, which affects the detention capacity of roof systems (Peng et al., 2019). The SWCC describes the substrate's ability to retain water as a function of matric suction, and is used to determine key parameters, including water retention capacity (WRC), permanent wilting point, and plant available water (De-Ville et al., 2017). The hydrological properties and performance of substrates are typically influenced by their physical characteristics, particularly pore size distribution, particle size distribution, and particle hydrophobicity (De-Ville et al., 2017; Hill et al., 2019). Optimizing substrate properties is essential to balance stormwater retention and detention while enhancing plant available water to support vegetation performance. Accurate and high-resolution measurements of hydraulic properties are critical as they provide key parameters for reliable hydrological modeling and large-scale simulations of green roof performance.

Biochar, a carbon-rich, porous material produced from pyrolyzed biomass, has been suggested as an ideal substrate additive for green roofs to enhance hydrological and vegetation performance (Cao et al., 2014; Liao et al., 2023; Lee & Kwon, 2024). Biochar amendment can

improve water retention and detention capacity (Huang et al., 2020; Gan et al., 2021; Tan & Wang, 2023), enhance plant available water content (Cao et al., 2014; Petreje et al., 2025), and reduce saturated (Huang et al., 2020; Gan et al., 2021) and unsaturated (Hussain & Ravi, 2021) hydraulic conductivity of substrates, primarily due to large specific surface area and high porosity of biochar and increased water flow tortuosity. In addition, biochar often exhibits a bimodal pore structure with pores at the nano- to micro-scale (Lu & Zong, 2018), which can influence water retention and infiltration processes in substrates. However, unprocessed biochar is lightweight and thus susceptible to wind and water erosion, particularly on highly exposed roof systems, potentially resulting in biochar loss and environmental pollution (Liao et al., 2022c).

Biochar granulation and particle size modification are important post-processing approaches suggested to enhance biochar physicochemical properties (Thomas, 2021) while mitigating biochar erosion loss (Liao et al., 2022c). We recently found that addition of granulated biochar to green roof substrates increased WRC by 26%, though this improvement was less pronounced than unprocessed biochar amendment due to lower porosity and hydrophobicity (Liao et al., 2022a). Granulated biochar has also been shown to reduce erosion losses of both biochar and non-biochar particles on green roof substrates (Liao et al., 2022c). However, no research has been done examining hydraulic properties of green roof substrates amended with granulated versus unprocessed biochars or the underlying mechanisms involved.

Application of relatively large biochar particles can potentially reduce biochar erosion losses due to increased particle mass, while enhancing hydraulic properties of the substrates. Coarse biochar particles may also better increase substrate WRC than fine biochar particles due to their higher intra-porosity and hydrophilicity (Wang et al., 2019; Edeh & Mašek, 2021). In

113 contrast, small biochar particles generally have large specific surface area and high intra-
114 porosity, thereby more effectively enhancing substrate WRC compared to large biochar particles
115 (Ibrahim et al., 2017). Moreover, the addition of fine biochar particles can increase water flow
116 tortuosity by clogging substrate pores, further improving WRC (Esmaeelnejad et al., 2017).
117 However, fine biochar particles may reduce air-filled porosity and water infiltration, resulting in
118 waterlogging of green roofs during and after intense rainfall events that requires additional
119 stormwater control measures (Werdin et al., 2021). Studies have also shown that the effects of
120 biochar particle size on hydraulic properties vary with soil particle size distribution (Razzaghi et
121 al., 2020). Green roof substrates are engineered media consisting of materials in various particle
122 sizes, which generally have different textures and hydraulic properties than natural soils (Liao et
123 al., 2023), highlighting the importance of designing appropriate biochar for green roof
124 applications. Research on the effects of biochar particle size on the hydraulic properties of green
125 roof substrates is lacking, in particular, accurate and high-resolution measurements of hydraulic
126 properties, including K and SWCC.
127 In the present study we investigated the effects of biochar type (granulated vs.
128 unprocessed biochars) and particle size (0.25–6.3 mm) on K and SWCC of green roof substrate
129 using accurate, high-resolution KSAT and HYPROP devices, respectively. To understand the
130 underlying mechanisms of biochar effects on substrate hydraulic properties, we also examined
131 specific surface area, pore structure and characteristics, and chemical functional groups of
132 biochars. The following hypotheses were tested: (1) unprocessed biochar will better increase
133 WRC and decrease K of substrates compared to granulated biochar due to higher macroporosity;
134 (2) small biochar particles will result in increased WRC and reduced K compared to large
135 biochar particles due to large specific surface areas; (3) intermediate-sized biochar particles will

136 better balance water retention and detention of substrates; (4) all biochar-substrate mixtures will
137 show a biphasic or multiphasic SWCC.
138
139 **2. Materials and methods**
140 ***2.1. Biochar and substrate preparation and characterization***
141 The two biochars used in this study were produced from conifer feedstock. Unprocessed
142 biochar was produced from conifer sawmill wastes with mixed particle sizes through slow
143 pyrolysis at 625 ˚C and a residence time of ~20 minutes (Titan Clean Energy Projects Co.,
144 Canada). Granulated biochar was produced from similar raw biochar through a drum granulation
145 process with ground unprocessed biochar and a proprietary binder. Unprocessed biochar was
146 sieved into particle size ranges of 0.25–0.5 mm, 0.5–1 mm, 1–2 mm, 2–2.8 mm, 2.8–4 mm,
147 while granulated biochar was sieved into 1–2mm, 2–2.8 mm, 2.8–4mm, and 4–6.3 mm. The
148 overlapping 1–4 mm particle size range was precisely controlled across both biochar types to
149 investigate biochar granulation effects. Unprocessed biochar was thermally treated at 100 ˚C for
150 24 hours to reduce phytotoxic compounds. A commercial green roof substrate (Gro-Bark, Inc.,
151 Canada) that follows FLL (Forschungsgesellschaft Lanschaftsentwicklung Landschaftsbau)
152 guidelines was used in this study. The substrate is classified as well-graded sand and consists of
153 70% porous aggregates, 25% composted organic matter, and 5% fine sand. Unprocessed and
154 granulated biochars in each particle size class were applied to the substrate at a dosage of 25 t/ha
155 (equivalent to ~4.5% w/w). Detailed information on biochar and substrate preparation,
156 characterization, and testing methods are documented in Liao et al. (2022a).
157 Scanning electron microscope (SEM) images were taken to qualitatively assess surface
158 structure and morphological features of unprocessed and granulated biochars using a Hitachi

159 Scanning Electron Microscope SU3500 (Hitachi Ltd., Japan). Representative biochar samples
160 were mounted on stubs with carbon tape and were sputter-coated with gold-palladium using a
161 sputter coater (Bal-Tec SCD 050, Bal-Tec, USA) to enhance conductivity. The surface
162 functional groups of biochar were characterized using Fourier transform infrared spectroscopy
163 (FTIR) with a Bruker Tensor 27 FTIR Spectrometer (Bruker, USA). Spectra were acquired in the
164 range of 4000 to 400 cm^{-1} at a resolution of 4 cm^{-1}, with 32 scans per sample. The samples were
165 prepared as compressed pellets from a homogenized mixture of 0.2 g potassium bromide (KBr)
166 and 0.25% of biochar ground with a mortar and pestle. Biochar was oven-dried at 65 ˚C for 12
167 hours prior to the measurements to remove moisture.
168 Nitrogen adsorption-desorption isotherms were determined at 77 K using a NOVA 1200e
169 surface area analyzer (Quantachrome Instruments, USA). Biochar specific surface area was
170 measured through the Brunauer–Emmett–Teller (BET) method with a relative pressure (P/P_0)
171 range of 0.01–0.3. The total pore volume of biochar was determined using a single nitrogen
172 adsorption point at $P/P_0 = 0.98$ (Sigmund et al., 2017). Biochar micropore volume was obtained
173 through the Dubinin-Radushkevich (DR) method and the mesopore volume was calculated as the
174 difference between total pore volume and micropore volume (Leng, 2021). The mesopore and
175 micropore diameter distribution of biochar was determined by the Barrett–Joyner–Halenda
176 (BJH) and Density Functional Theory (DFT) methods (Bardestani et al., 2019; Leng, 2021).
177 Biochar was degassed at 150 °C for 20 hours prior to the measurements. The data were analyzed
178 in NOVAWin software (Quantachrome Instruments, USA) to obtain the specific surface area,
179 pore volume, and pore size distribution of biochar. Duplicate measurements were conducted for
180 unprocessed and granulated biochars in each particle size range.
181

2.2. Hydraulic property measurements

2.2.1. Soil-water characteristic curve and unsaturated hydraulic conductivity

The soil-water characteristic curve (SWCC) and unsaturated hydraulic conductivity (K_{unsat}) of the substrate and biochar-substrate mixtures were determined using a HYPROP device (METER Group, Germany). The HYPROP system measures the soil water retention and release processes using an evaporation method (Peters & Durner, 2008; Peters, 2013). The substrate and biochar-substrate mixtures were packed into the HYPROP sample ring (volume = 250 cm^3, height = 5 cm, inside diameter = 8 cm). The samples were saturated in deionized, degassed water from bottom to top in a container for 24 hours prior to measurements. The samples were mounted on the HYPROP instrument with two tensiometers positioned at heights of 1.75 cm and 3.75 cm to measure matric suction, while a connected HYPROP balance simultaneously recorded mass changes throughout the evaporation process. Samples were measured at room temperature (20 to 25 ˚C, with an average temperature of 23˚C). The HYPROP measurements were terminated when cavitation occurred in both tensiometers. The dry mass of the samples was determined by oven-drying at 105 ˚C for 24 hours. Each sample measurement lasted an average of 24 days, ranging from a minimum of 11 days (pure substrate) to a maximum of 32 days (biochar-amended substrates). Duplicate measurements were conducted for each substrate and biochar-substrate mixture.

The HYPROP-FIT software (METER Group, USA) was used to analyze data from the evaporation experiments and to fit K_{unsat} following the HYPROP-FIT manual (Pertassek, et al., 2015). The data were fitted with the Peters–Durner–Iden (PDI) expression (Peters, 2013; Iden & Durner, 2014) of the bimodal constrained van Genuchten (VGbi-PDI) model (Van Genuchten, 1980; Haghverdi et al., 2020), which accounts for bimodal pore structure. Model fits were

assessed using the root mean square error (RMSE) and sample-sized adjusted Akaike Information Criterion (AICa) values. The PDI variant was employed to capture the full SWCC, including the dry-end, due to its improved accuracy and reliable model performance even without direct dry-end measurements (Haghverdi et al., 2020). The general form of the PDI retention model is expressed as the sum of capillary and adsorptive water retention (Peters, 2013; Iden & Durner, 2014):

$$\theta(h) = (\theta_s - \theta_r)S_{cap}(h) + \theta_r S_{ad}(h) \quad (1)$$

where θ is the volumetric water content (m^3/m^3), h is the matric suction (cm), θ_s is the saturated water content (m^3/m^3), θ_r is the maximum water content for water adsorption (m^3/m^3), and S_{cap} and S_{ad} are the saturation of capillary and adsorptive water retention (m^3/m^3), respectively.

The capillary scaling function S_{cap} of the PDI variant is calculated as:

$$S_{cap}(h) = \frac{\Gamma(h)-\Gamma_0}{1-\Gamma_0} \quad (2)$$

where Γ_0 is the basic function at h = h_0. The adsorptive scaling function is calculated as:

$$S_{ad}(x) = 1 + \frac{1}{x_a - x_0}\left\{x - x_a + bln\left[1 + \exp\left(\frac{x_a - x}{b}\right)\right]\right\} \quad (3)$$

where x = pF = $\log_{10}$ (h, cm), x_a = $\log_{10}$ (h_a, cm), with h_a being the suction at air entry for the adsorptive retention, and x_0 = $\log_{10}$ (h_0, cm), with h_0 being the suction where the water content is 0. The value of $h_0 = 10^{6.8}$ cm was used to represent the section at oven dryness for 105 ˚C. The smoothing parameter b is dependent on the capillary scaling function S_{cap} and is given by:

$$b = 0.1 + \frac{0.2}{n^2}\left\{1 - exp\left[-\left(\frac{\theta_r}{\theta_s - \theta_r}\right)^2\right]\right\} \quad (4)$$

where n is an empirical curve shape parameter. The bimodal constrained van Genuchten model is a weighted sum of the unimodal van Genuchten functions, expressed as:

$$\Gamma(h) = \sum_{i=1}^{2} w_i \left[\frac{1}{1+(\alpha_i h)^{n_i}}\right]^{m_i} = \sum_{i=1}^{2}(w_i \Gamma_i) \quad (5)$$

where Γ is the effective saturation ranging from 0 to 1, h is the matric suction (cm), w_i is the weighting factor that $\sum w_i = 1$, and α_i, n_i, and m_i are empirical curve shape parameters, with $m_i = 1 - n_i^{-1}$.

The unsaturated hydraulic conductivity (K_{unsat}) is calculated as:

$$K = K_s\left[(1-\omega)K_{rel}^{cap}(S_{cap}) + \omega K_{rel}^{film}(S_{ad})\right] \quad (6)$$

where K is the unsaturated hydraulic conductivity, K_s is the saturated conductivity, ω is a weighting factor that $\sum w_i = 1$, K_{rel}^{cap} is the relative conductivity associated with capillary flow, and K_{rel}^{film} is the relative conductivity associated with film flow, as shown below:

$$K_{rel}^{cap} = \left(\sum_{i=1}^{2} w_i S_{cap_i}\right)^{\tau}\left[1 - \frac{\sum_{i=1}^{2} w_i \alpha_i \left(1-\Gamma_i^{1/m_i}\right)^{m_i}}{\sum_{i=1}^{2} w_i \alpha_i \left(1-\Gamma_0^{1/m_i}\right)^{m_i}}\right]^2 \quad (7)$$

$$K_{rel}^{film} = \left(\frac{h_0}{h_a}\right)^{a(1-S_{ad})} \quad (8)$$

where τ is the tortuosity and connectivity parameter and the parameter a is the slope on the log-log scale, which is set to –1.5 (Peters, 2013).

The field capacity and permanent wilting point of the samples were determined as water retention at pF = 2.5 (~ 33 kPa) and pF = 4.2 (~ 1500 kPa), respectively (Cassel & Nielsen, 1986). Plant available water content was calculated as the difference between field capacity and permanent wilting point (Cassel & Nielsen, 1986).

2.2.2. Pore size distribution of substrates and biochar-substrate mixtures

The pore size distribution of the substrate and biochar-substrate mixtures was derived from the sample water retention data at matric potentials of approximately −3, −6, and −33 kPa, which correspond to pore diameters of 100, 50, and 9 μm, respectively (Edeh & Mašek, 2021). Pore volume fractions were estimated from variations in volumetric water content, using

249 designated pore diameter ranges to define class boundaries. Macro-porosity, meso-porosity, and
250 micro-porosity corresponded to the volume fractions of pores with radii greater than 100 μm,
251 between 50 and 100 μm, and less than 50 μm, respectively (Edeh & Mašek, 2021).
252
253 ***2.2.3. Saturated hydraulic conductivity***
254 Saturated hydraulic conductivity (K_{sat}) was measured using a KSAT device (METER
255 Group, USA) with a 2-cm constant head and 1-second measurement intervals. The K_{sat} was
256 determined using the Darcy's law:
257 $$K_{sat} = \frac{Q}{A} \times \frac{L}{H} \quad (9)$$
258 where Q is the steady-state flow rate from a Mariotte flask, A is the cross-sectional area of the
259 substrate sample, L is the length of the substrate sample, and H is the hydraulic head difference
260 between inlet and outlet level. K_{sat} of the samples was normalized to 10 ˚C by accounting for the
261 temperature dependence of water viscosity (Gao & Shao, 2015). The substrate and biochar-
262 substrate mixtures were saturated with deionized water for 24 hours prior to the measurements.
263 Triplicate samples were analyzed for each substrate and biochar-substrate mixture, with each
264 sample measured ten times.
265
266 **2.3. Statistical analysis**
267 The effects of biochar processing method and particle size on surface area and pore
268 characteristics of biochars, as well as the hydraulic properties of the substrate and biochar-
269 substrate mixtures, were analyzed using one-way analysis of variance (ANOVA). Two-way
270 ANOVA was performed for the subset of factorial treatments (granulated and unprocessed
271 biochars in particle size ranges of 1–2 mm, 2–2.8 mm, and 2.8–4 mm) to examine the biochar

type by particle size interactions. Post-hoc Tukey's HSD tests were conducted for ANOVA results that were significant. *t*-tests were performed to determine whether each biochar treatment was statistically different from the pure substrate. *P*-values were adjusted using the false discovery rate procedure for multiple comparisons (Benjamini & Hochberg, 1995). All statistical analyses and data visualization were conducted in R version 4.4.1 (R Core Team, 2024).

3. Results

3.1. Biochar physicochemical properties

3.1.1. Biochar pore structure and functional groups

The SEM images showed that unprocessed biochar was well-structured, with the pores corresponding to the wood cells of the conifer feedstock (Fig. 1a). In contrast, the pore structure of the granulated biochar collapsed during the granulation process (Fig. 1b). In addition, granulated biochar exhibited a non-uniform, fractured surface morphology and was composed of biochar particles of varying sizes (Fig. 1b).

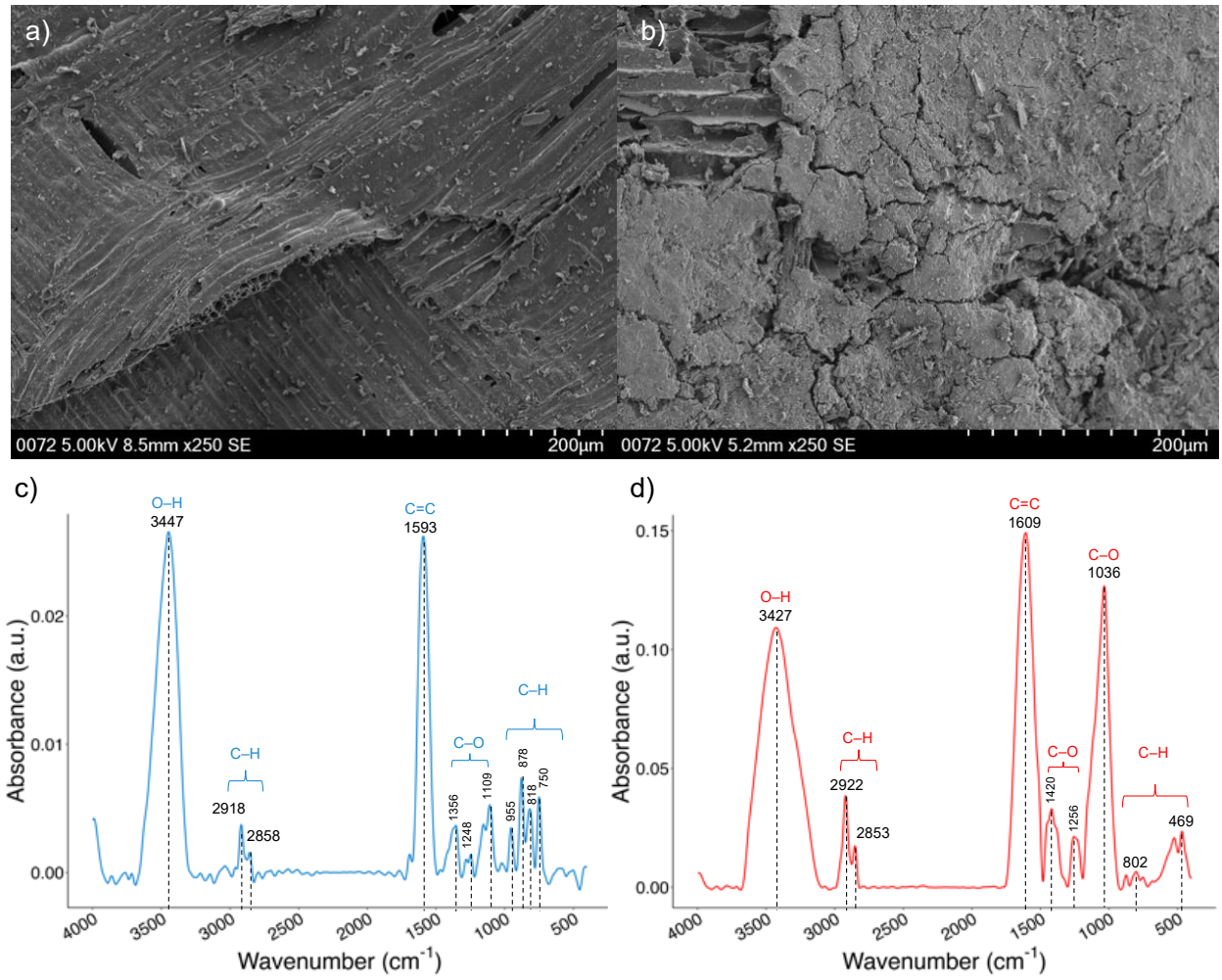

Fig. 1. Scanning electron microscope (SEM) images for unprocessed (a) and granulated (b) biochars at the magnification of 250 ×, and Fourier-transform infrared spectroscopy (FTIR) spectra of unprocessed (c) and granulated (d) biochars. Dashed lines indicate peaks of FTIR spectra. Unprocessed and granulated biochars are shown in blue and red colors, respectively.

The FTIR spectra of unprocessed (Fig. 1c) and granulated (Fig. 1d) biochars revealed characteristic absorbance bands associated with organic and oxygen-containing functional groups. In the unprocessed biochar, a broad absorption band at 3447 cm^{-1} was attributed to O–H stretching vibrations of hydroxyl groups. A prominent peak at 1593 cm^{-1} was assigned to aromatic C=C stretching. Additionally, weak absorption bands at 2918 cm^{-1} and 2858 cm^{-1} were related to C–H bonds. The FTIR spectrum of the granulated biochar exhibited similar strong

298 bands at 3427 cm^{-1} and 1609 cm^{-1}, corresponding to O–H and aromatic C=C stretching
299 vibrations, respectively. The C–H stretching peaks were also present at 2922 cm^{-1} and 2853 cm^{-1}.
300 Notably, a distinct and sharp peak at 1036 cm^{-1} appeared in the granulated biochar, which
301 corresponds to C–O stretching vibrations. Several weak bands related to C–O and C–H
302 stretching vibrations were also observed in both unprocessed and granulated biochars, indicating
303 the presence of residual oxygenated functional groups and aliphatic linkages.
304
305 *3.1.2. Biochar specific surface area and pore characteristics*
306 Unprocessed biochars had a greater mean BET specific surface area (95 ± 30 m^2/g [mean
307 ± SE]) than granulated biochars (23 ± 9 m^2/g) for the particle size ranges where these overlapped
308 (i.e., 1–2 mm, 2–2.8 mm, 2.8–4 mm) ($p < 0.05$) (Table 1). There were also strong interactive
309 effects (Table 1): BET specific surface areas of unprocessed biochars increased with decreasing
310 biochar particle sizes ($p < 0.05$), with the unprocessed biochar at 0.5–1 mm (262 ± 6 m^2/g) and
311 2.8–4 mm (13 ± 3 m^2/g) showing the highest and lowest BET specific surface areas, respectively,
312 while there was no particle size effect with granulated biochar (Fig. 2a; Table 2). Likewise,
313 unprocessed biochars (0.066 ± 0.017 cm^3/g) had a higher total pore volume than granulated
314 biochars for the overlapping particle sizes (0.028 ± 0.008 cm^3/g), with significant interactive
315 effects of biochar type and particle size ($p < 0.05$) (Fig. 2b; Table 1). The total pore volume of
316 unprocessed biochars generally declined with biochar particle size (Fig. 2b), with the
317 unprocessed biochars at 0.5–1 mm (0.154 ± 0.011 cm^3/g) and 2.8–4 mm (0.017 ± 0.002 cm^3/g)
318 showing the highest and lowest total pore volumes, respectively (Fig. 2b; Table 2). However, no
319 particle size effect on BET specific surface area or total pore volume was observed for the
320 granulated biochars. Similar patterns were observed for the biochar micropore volume (Fig. S1

and Table 2). Overall, unprocessed biochars (86.4%) had a higher percentage of micropores than granulated biochars (60.7%), while granulated biochars presented higher percentage of mesopore (29.3%) than unprocessed biochars (13.6%) (Fig. S1 and Table S1).

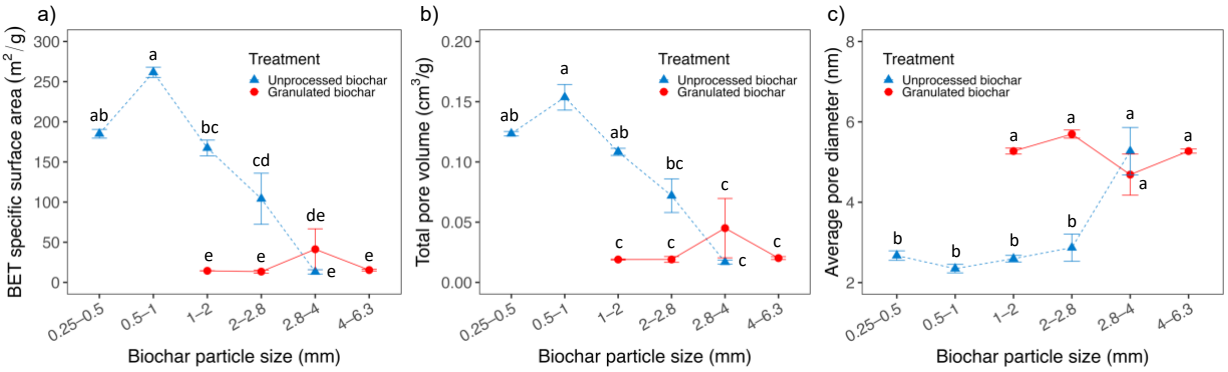

Fig. 2. BET specific surface area (a), total pore volume (b), and average pore diameter (c) of unprocessed and granulated biochars across different particle size ranges. Means are plotted ± 1 SE based on duplicate measurements for each biochar. Dots with different lowercase letters differ significantly at $p < 0.05$ according to Tukey's HSD test. Unprocessed and granulated biochars are shown in blue and red colors, respectively.

Biochar pore size distributions were also estimated from gas sorption data. Granulated biochars had a larger estimated average pore diameter (5.22 nm) than unprocessed biochars (3.58 nm) for the overlapping particle sizes, with biochar type and biochar particle size showing interactive effects ($p < 0.05$) (Table 1). Unprocessed biochars presented significant particle size effects, with the 2.8–4 mm fraction showing the largest average pore diameter of 5.27 ± 0.59 nm, while no differences were observed among the other particle size ranges (Fig. 2c). Additionally, granulated biochars exhibited a larger mean DFT pore diameter (2.92 ± 0.08 nm), indicative of microporous structure, compared to unprocessed biochars (1.90 ± 0.03 nm) (Fig. S2; Table S1). No particle size effect on average pore diameter or DFT pore diameter was found for the granulated biochars.

Consistent with the pore volume and diameter results, the pore size distribution indicated that unprocessed biochars generally presented greater pore volumes across 3–30 nm ranges (Fig. 3). Moreover, unprocessed biochars exhibited a high concentration of small pores around ~2 nm in diameter (Fig. 3a). In contrast, granulated biochars showed a highly variable pore size distribution with relatively low pore volumes across the 2–20 nm range (Fig. 3b).

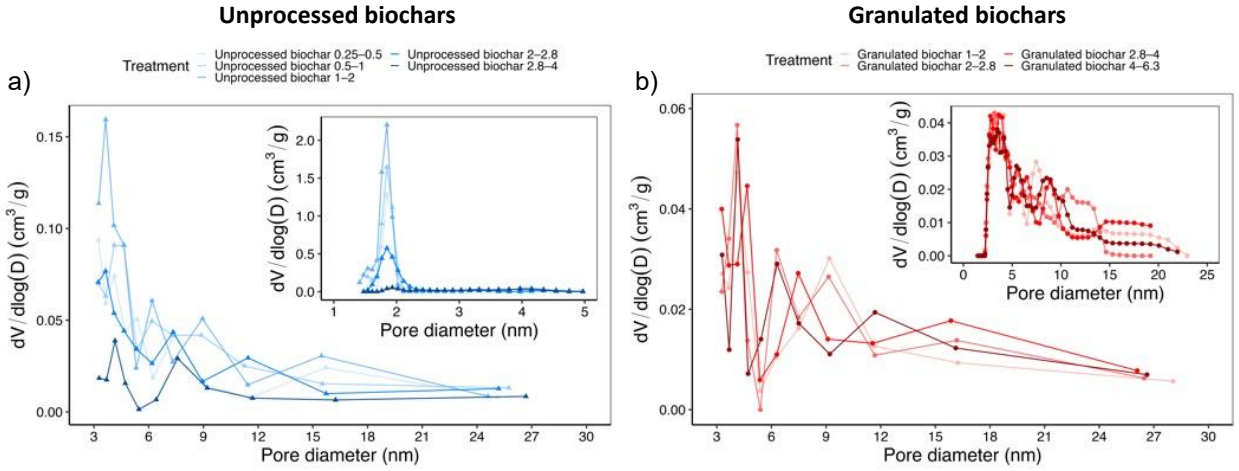

Fig. 3. Pore size distribution of unprocessed (a) and granulated (b) biochars across different particle size ranges. Mesopore diameter distributions, determined by the Barrett–Joyner–Halenda (BJH) method, are shown in the main panels, while micropore diameter distributions, derived from Density Functional Theory (DFT), are presented in the embedded insets.

3.2. Soil-water characteristic curves and hydraulic properties

Biochar post-processing and particle size affected water retention and release behavior of the substrates, highlighting their important roles in influencing hydrological performance and stormwater management of green roofs (Fig. 4). The water retention and release processes of biochar-amendment substrates were best described by the PDI variant of the bimodal constrained van Genuchten (VGbi-PDI) model, indicating the presence of a bimodal pore structure in the biochar-substrate mixtures. The water retention of substrates increased from 0 pF to 2.5 pF with the addition of unprocessed and granulated biochars across all particle size ranges, except for the

2.8–4 mm biochars (Fig. 4). The increase was more pronounced with unprocessed biochars. In addition, substrates amended with unprocessed biochars in the 0.25–2.8 mm particle size range showed sharper declines in water content between 0.5 pF and 2.5 pF compared to those amended with granulated biochars (Fig. 4). The fitted parameter values for the VGbi-PDI models were describe in Table S2. The SWCC in kPa was shown in Fig. S3.

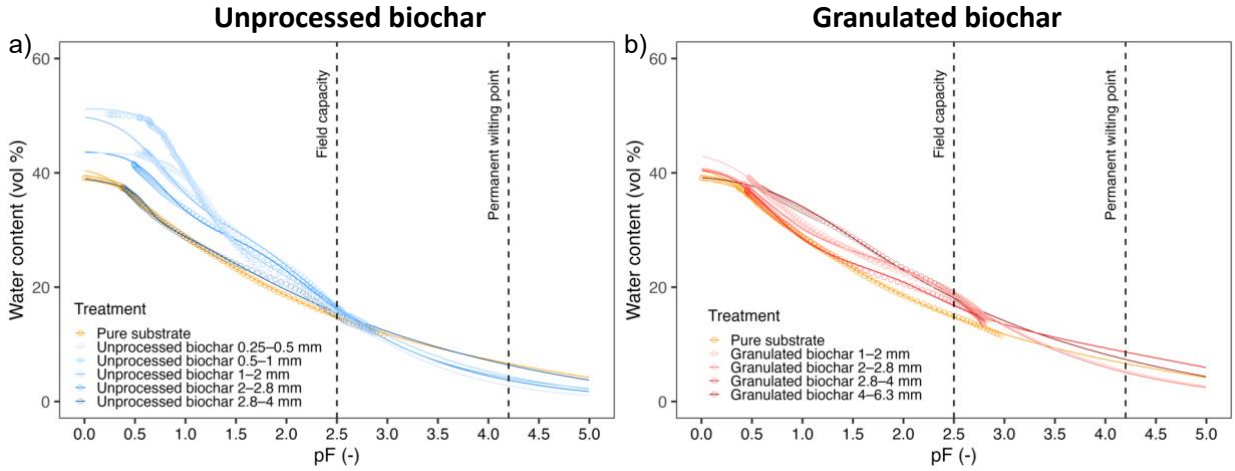

Fig. 4. Soil-water characteristic curves for the pure substrate (a–b) and the substrates amended with unprocessed (a) and granulated (b) biochars in different particle size ranges. Open symbols represent the measurement data from the HYPROP device. Lines represent the fitted PDI variant of the bimodal constrained van Genuchten model for one representative replicate. Dashed lines indicate field capacity at 2.5 pF and permanent wilting point at 4.2 pF. Blue and red colors indicate unprocessed and granulated biochars, respectively, with the darker colors presenting larger particle size ranges. Orange color indicates the pure substrate.

The substrates with granulated biochar addition (18%) showed significantly higher mean field capacity compared to those amended with unprocessed biochars (16%) and those without biochar (15%) (Fig. 5a and Table 3). In addition, the granulated biochar-amended substrates (7.4%) had a higher permanent wilting point than the unprocessed biochar-amended substrates (5.0%) ($p < 0.05$) (Fig. 5b and Table 3). However, biochar post-processing showed no effect on plant available water of substrates (Fig. 5c and Table 3). Biochar particle size effects on field capacity and plant available water were observed within the overlapping size ranges, with the

biochars in the 1–2 mm and 2–2.8 mm categories better increasing mean field capacity and plant available water than the 2.8–4 mm biochar ($p < 0.05$) (Fig. 5 and Table 3). In addition, the substrate with the amendment of unprocessed biochar in 0.5–1 mm had higher plant available water than that with the granulated biochar in 2.8–4 mm (Fig. 5c). The substrates amended with 0.25–0.5 mm and 1–2 mm unprocessed biochars and 1–2 mm and 2–2.8 mm granulated biochars had higher field capacity than the pure substrate ($p < 0.05$). Moreover, the addition of 0.5–1 mm and 2–2.8 mm unprocessed biochars increased the substrate plant available water compared to the control ($p < 0.05$).

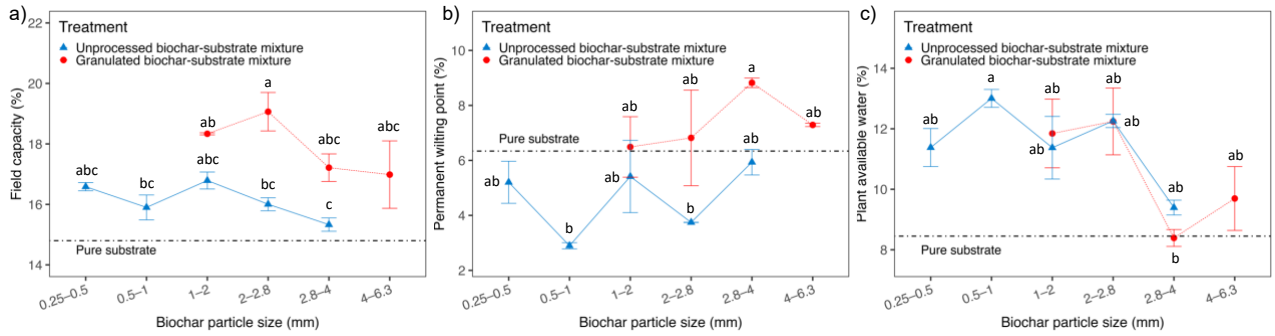

Fig. 5. Field capacity (a), permanent wilting point (b), and plant available water (c) for the pure substrate and the substrates amended with unprocessed and granulated biochars. Blue and red labels represent unprocessed and granulated biochars, respectively. Dashed lines indicate the pure substrate. Means are plotted ± 1 SE for each biochar treatment and the pure substrate. Dots with different lowercase letters differ significantly at $p < 0.05$ according to Tukey's HSD test.

3.3. Hydraulic conductivity

Unprocessed and granulated biochars showed strong particle size effects on saturated hydraulic conductivity (K_{sat}) (Tables 3 and S3). The K_{sat} of the biochar-substrate mixtures increased with the increasing unprocessed biochar particle sizes, with the biochar in the 2.8–4 mm category showing the highest K_{sat} (15570 cm/day) (Fig. 6). The addition of granulated biochar in the 2–2.8 mm size range resulted in a greater increase in K_{sat} compared to the 4–6.3 mm granulated biochar (Fig. 6). Biochar type and particle sizes showed interactive effects on

403 K_{sat}, indicating that biochar particle size effect differed between unprocessed and granulated
404 biochars (Table 3). Overall, biochars in the 1–2 mm particle size range showed a lower K_{sat} than
405 those in the 2–2.8 mm and 2.8–4 mm ranges (Table 3). In addition, the substrates amended with
406 the unprocessed biochars in 0.25–0.5 mm, 0.5–1 mm, and 1–2 mm particle size ranges had lower
407 K_{sat} than the pure substrate ($p < 0.05$). No difference was observed in substrate K_{sat} for the pure
408 substrate or the substrates amended with the unprocessed biochars and granulated biochars ($p >$
409 0.05) (Table 3).

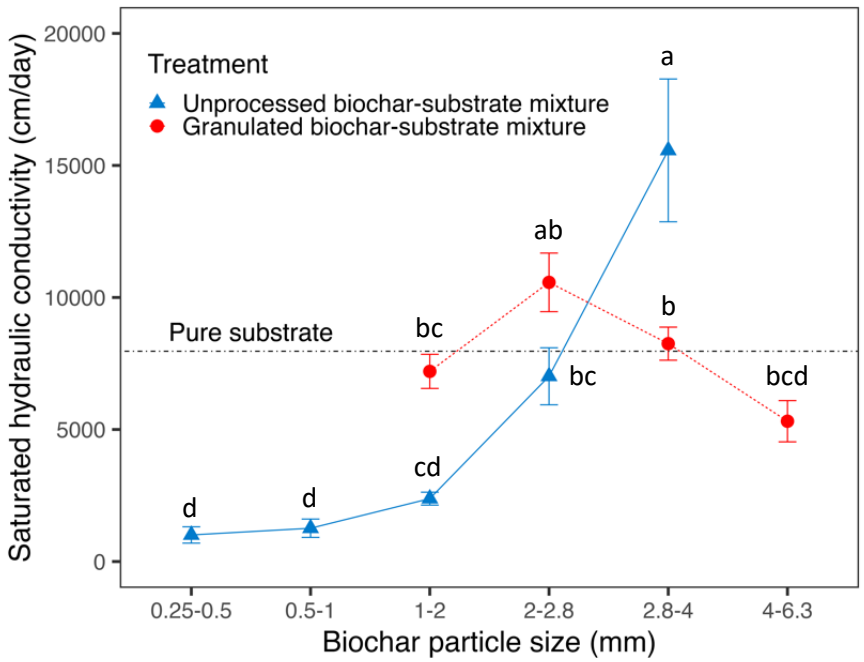

410

411 **Fig. 6.** Saturated hydraulic conductivity (K_{sat}) for the pure substrate and the substrates amended
412 with unprocessed and granulated biochars in different particle size ranges. Blue and red labels
413 represent unprocessed and granulated biochars, respectively. Dashed lines indicate the pure
414 substrate. Means are plotted ± 1 SE for each biochar treatment and the pure substrate. Dots with
415 different lowercase letters differ significantly at $p < 0.05$ according to Tukey's HSD test.

416

417 The addition of biochars slightly increased the substrate unsaturated hydraulic
418 conductivity (K_{unsat}) for pF < 2.5, except for the unprocessed biochar in 0.5–1 mm and 2.8–4 mm

(Fig. 7). However, the effects were not significant. In addition, no biochar effect on K_{unsat} were observed for pF > 2.5.

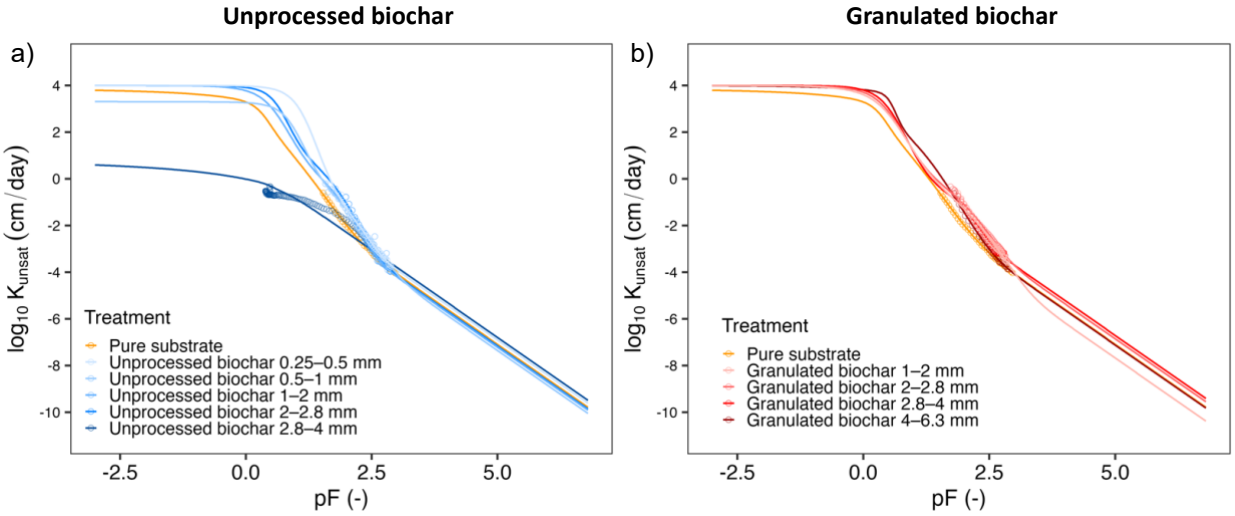

Fig. 7. Unsaturated hydraulic conductivity curves for the pure substrate (a–b) and the substrates amended with unprocessed (a) and granulated (b) biochars in different particle size ranges. Open symbols represent measurement data obtained from the HYPROP device, while solid lines indicate model fits for one representative replicate. Blue and red colors indicate unprocessed and granulated biochars, respectively, with the darker colors presenting larger particle size ranges. Orange color indicates the pure substrate.

3.4. Pore size distribution of the substrate and biochar-substrate mixtures

Biochar applications altered the pore size distribution and total porosity of the green roof substrates. The addition of unprocessed and granulated biochars increased the total porosity of the pure substrate by 8.3% and 7.4%, respectively (Fig. 8a). The amendment of unprocessed and granulated biochars increased the substrate microporosity by 40% and 8%, respectively, compared to the pure substrate (Fig. 8b). On average, substrates with the unprocessed biochars (3.7%) had higher proportion of mesopores than those amended with the granulated biochars (2.3%) and the pure substrate (3.0%) (Fig. 8c). The substrate with intermediate-sized and small-sized granulated biochars reduced the substrate mesoporosity (Fig. 8c). In contrast, the addition

of granulated biochars reduced the substrate macroporosity to 16%, whereas unprocessed biochars had a negligible effect on substrate microporosity (Fig. 8d).

Substrates amended with unprocessed biochars of small (0.25–0.5 mm) and large (2–2.8 mm and 2.8–4 mm) particle sizes exhibited lower macroporosity compared to those with intermediate particle sizes (0.5–1 mm and 1–2 mm) (Fig. 8d). In contrast, mesoporosity generally increased with decreasing unprocessed biochar particle size (Fig. 8c). No consistent pattern in pore size distribution was observed for the substrates amended with granulated biochars.

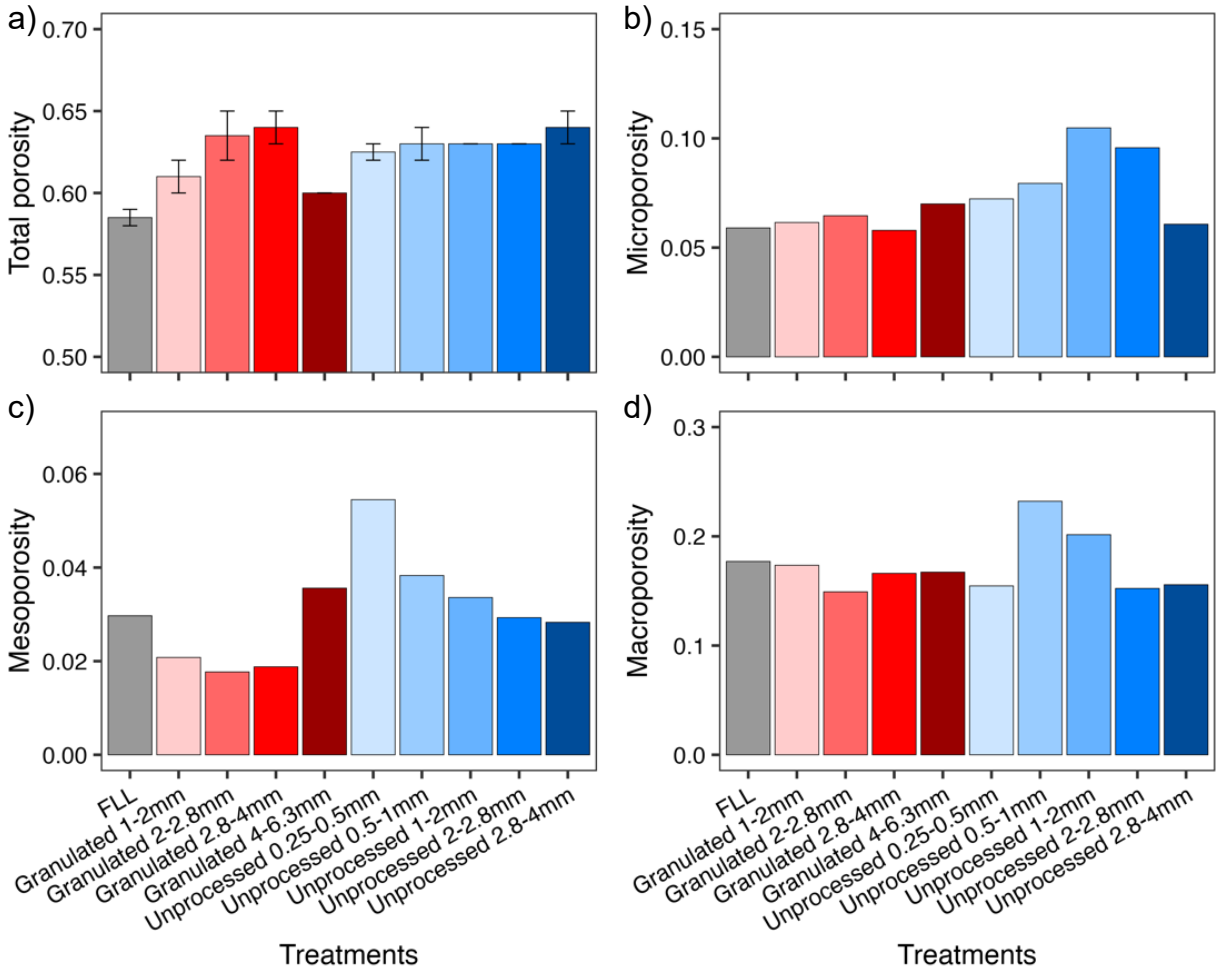

Fig. 8. Pore size distribution and total porosity of the pure substrate and the substrate amended with unprocessed and granular biochars. Pore size distribution was derived from HYPROP measurements for one representative replicate. Mean total porosity is plotted ± 1 SE and is shown based on duplicate measurements for each biochar treatment and the pure substrate.

4. Discussion

4.1. Biochar post-processing affects biochar surface and pore characteristics

Our results showed that unprocessed biochars present well-structured pores. In contrast, granulated biochars exhibit non-uniform and fractured surface morphology, along with reduced porosity and lower BET specific surface area. This is likely attributable to the collapse of physical macropore structure during processing (Fig. 1ab) and the presence of binding agents during the granulation process, which likely occluded pores and decreased the overall porosity of the granulated biochar (Liao et al., 2022a). In addition, granulated biochars exhibited more uniform and consistent BET specific surface area and pore structure across different particle sizes compared to unprocessed biochars. Minimal particle size effects were observed for granular biochars, likely due to the uniformity of biochar granulation process, which preserves the biochar's internal structure regardless of particle size (Bowden-Green & Briens, 2016; Briens & Bowden-Green, 2019). In contrast, the BET specific surface area and pore characteristics of unprocessed biochars varied strongly with biochar particle size. As particle size decreased, the BET specific surface area and total pore volume increased, possibly due to the greater exposure of inner pores (Fahmi et al., 2018). These trends are consistent with the previous findings in natural soils (Jaafar et al., 2015; Fahmi et al., 2018). The enhanced BET specific surface area and total pore volume in smaller biochar particles may enhance water and nutrient retention on green roofs (Liao et al., 2022b). Our results also showed that biochar addition increased the total porosity of green roof substrates, particularly the proportion of micropores, due to the large BET specific surface area and pore volume of biochars.

Unprocessed biochars had smaller average pore diameters than granulated biochars, presenting higher microporosity. This can be attributed to the intrinsic microporous structure of the conifer feedstock (Lu & Zong, 2018). The high concentration of micropores (< 2 nm) presented in the unprocessed biochars can contribute to high biochar water retention capacity (Liao et al., 2022a). In contrast, granulated biochars showed highly variable pore size distributions and relatively low pore volume across micropore and mesopore scales, which may result from collapsed pore structures and non-uniform surface morphologies introduced during the granulation process (Bowden-Green & Briens, 2016), as evidenced by the SEM images (Fig. 1ab). The alteration of pore characteristics during biochar granulation has been shown to reduce biochar water retention capacity compared to unprocessed biochar (Liao et al., 2022a).

The FTIR spectra revealed that granulated biochar exhibited stronger hydrophilic character than unprocessed biochar, as indicated by the distinct C–O stretching band at 1036 cm^{-1} and the pronounced O–H and C=C peaks (Fan et al., 2022). The distinct FTIR spectra of granulated biochars may reflect either oxidation during processing or the chemistry of the binding agent. These oxygen-containing functional groups enhance water affinity (Fan et al., 2022) and pollutant adsorption capacity (Fahmi et al., 2018; Dai et al., 2021), suggesting that granulated biochars may improve water retention and contaminant removal performance. The presence of distinct functional groups, particularly the C–O peak, in the granulated biochar is likely due to the proprietary organic binding agents used during granulation processes (Hu et al., 2015; Dos Santos Júnior et al., 2025), although oxidation during processing may also contribute. In contrast, the relatively weak C–O signal in unprocessed biochar implies reduced surface polarity and lower hydrophilicity (Fan et al., 2022). This is consistent with previous study

indicating the moderate hydrophobicity of wood-derived granulated biochar (Briens & Bowden-Green, 2019).

4.2. Biochar improves substrate hydraulic properties

Consistent with the effects of post-processing on biochar surface and pore characteristics, the addition of granulated biochar had more uniform effects on substrate hydraulic properties across particle size ranges compared to unprocessed biochars, consistent with the more homogeneous structure generated during the granulation process. The application of granulated biochar increased substrate field capacity, potentially enhancing stormwater retention on green roofs. This is likely due to the large BET specific surface area, high total pore volume, and hydrophilicity of the granulated biochar (as evidenced by the presence of oxygen-containing functional groups). These findings are consistent with the previous study that reported increased substrate water retention capacity following granular biochar amendment (Liao et al., 2022a). Likewise, a recent review indicated that biochar amendment improves hydraulic properties primarily in sandy soils, particularly under laboratory conditions where uniform homogenization of biochar-soil mixtures is ensured (Rabbi et al., 2021). The pronounced biochar effects on hydraulic properties observed in our study are likely enhanced by the coarse-textured nature of the green roof substrates, which are similar to coarse sandy soils. However, granulated biochar-substrate mixtures exhibited higher permanent wilting points than those amended with unprocessed biochar, suggesting that a larger proportion of the retained water was tightly bound within biochar intrapores and therefore less available to plants. Consequently, our results also showed that granulated biochar amendment had no effect on substrate plant available water. This finding contrasts with previous studies that reported increased plant available water and extended

518 days to permanent wilting point following unprocessed biochar application (Cao et al., 2014;
519 Petreje et al., 2025).

520 Our results indicate that the addition of fine biochar particles more effectively improved
521 substrate field capacity compared to coarse biochar particles, possibly due to the increased BET
522 specific surface area (Fig. 1) and micropores (Fig. S1) associated with smaller particle sizes, as
523 well as the clogging of inter-pores by fine biochar particles (Esmaeelnejad et al., 2017). The
524 amendment of 0.5–1 mm and 2–2.8 mm unprocessed biochars significantly increased the
525 substrate plant available water, likely due to the greater amount of mesopores (Fig. 8), which are
526 typically associated with plant available water storage (Edeh & Mašek, 2021). Higher plant
527 available water can enhance plant performance on green roof substrates (Petreje et al., 2025),
528 particularly for drought-sensitive species or during prolonged drought periods. In contrast,
529 although the substrate amended with 0.25–0.5 mm unprocessed biochar exhibited a relatively
530 high proportion of mesopores, it did not improve plant available water, highlighting the critical
531 role of biochar intrapores in regulating water retention and release dynamics that influence plant
532 available water (Edeh & Mašek, 2021). This finding contradicts prior studies that reported higher
533 soil plant available water with the addition of smaller-sized biochar (Alghamdi et al., 2020;
534 Werdin et al., 2021), possibly due to differences in the matrix substrate and the specific biochar
535 particle size ranges used.

536 All biochar-amended substrates were best described by the PDI variant of the bimodal
537 constrained van Genuchten model using the HYPROP-FIT software, indicating the presence of a
538 bimodal pore structure. This likely resulted from the combination of intrapores within the
539 biochar particles and interpores formed between biochar and substrate particles. Forms of the van
540 Genuchten model (Edeh & Mašek, 2021; Zhang et al., 2021) or the bimodal Durner model

(Trifunovic et al., 2018; Zanutel et al., 2024) have most often been fit to characteristic water release curves of biochar-amended soils. However, the highly porous structure of biochar, particularly granulated biochar composed of varying particle sizes and binding agents, can generate a complex pore network comprising intrapores at a range of spatial scales as well as interpores formed between particles (Zhao et al., 2023). A recent modeling study of soil hydrological processes across nearly 1,000 soil samples showed that soils often exhibit a bimodal pore size distribution due to particle aggregation (Shi et al., 2026), suggesting a strong tendency toward multimodal pore size distributions in biochar-amended substrates. As such, trimodal or multi-modal models may more accurately capture the pore architecture and hydraulic behavior of biochar-amended substrate (Zhao et al., 2023), particularly those containing granulated biochars.

Our results showed that K_{sat} decreased with decreasing unprocessed biochar particle size, particularly in the 0.25–0.5 mm, 0.5–1 mm, and 1–2 mm size ranges, likely due to the clogging of substrate interpores by fine biochar particles, which reduces effective pore space and increases water flow tortuosity (Edeh & Mašek, 2021). This suggests that fine unprocessed biochar particles may enhance the detention capacity of green roof substrates by reducing water flow rates and delaying peak discharge during rainfall events, particularly under saturated conditions. However, the reduced infiltration rates associated with the amendment of fine unprocessed biochar particles, especially those in the 0.25–0.5 mm and 0.5–1 mm ranges, may increase the risk of waterlogging during and after intense precipitation events, necessitating additional stormwater control measures (Werdin et al., 2021). The waterlogging associated with small biochar particles may also enhance methane emissions from green roofs (Halim et al., 2022). In contrast, the largest size class of unprocessed biochar (2.8–4 mm) most effectively increased K_{sat}, likely due to the increased interpores between particles formed by the elongated-shaped

564 unprocessed biochar (Liao & Thomas, 2019). However, a reduction in K_{unsat} was observed with
565 the addition of large unprocessed biochars, suggesting reduced water infiltration rates under
566 unsaturated conditions, potentially due to increased water retention associated with their
567 hydrophilic surfaces and higher intraporosity (Edeh & Mašek, 2021). In general, intermediate
568 biochar particle sizes can provide a balanced infiltration rate, thereby improving green roof
569 stormwater retention and detention capacity.
570
571 **4.3. Importance and future directions**
572 This study is the first to investigate the effects of biochar granulation on the hydraulic
573 properties of green roof substrates, providing critical insights for optimizing green roof substrate
574 design to improve stormwater management. The stable and uniform surface and pore
575 characteristics and hydrological properties of granulated biochar, combined with the strong
576 erosion resistance (Liao et al., 2022), highlight its high potential to improve the
577 multifunctionality of green roofs, including improved stormwater management, water quality
578 (Liao et al., 2022b), and plant performance (Liao et al., 2022a). Although the application of
579 unprocessed biochars in 0.5–1 mm and 2–2.8 mm particle size ranges increases plant available
580 water, intermediate-sized biochar (i.e., 2–2.8 mm) is recommended for green roofs to minimize
581 human exposure to fine dusts and to reduce erosion losses and risks of periodic waterlogging
582 (Tang et al., 2023). Granulation of fine biochar particles offers an effective solution for utilizing
583 biochar powders generated during production, which are often unsuitable for field applications
584 due to their high erodibility while enhancing the profitability of biochar production by enabling
585 the industrial-scale use of low-value biochar powders. In addition, our study provides essential
586 parameters for hydrological modeling, enabling a better mechanistic understanding of biochar

effects on hydrological performance and stormwater management under different conditions, including future climate scenarios. When combined with geospatial analysis and stormwater modeling tools, such as Storm Water Management Model (SWMM), these findings support the evaluation and optimization of stormwater management strategies across large spatial and temporal scales.

It should be emphasized that the present study presents a short-term experimental data on freshly prepared biochar-substrate mixtures. The hydraulic properties of green roof substrates are likely to evolve over time due to changes in substrate physicochemical characteristics, including shifts in particle and pore size distributions, organic matter accumulation or depletion, and plant-biochar-soil interactions, such as aggregation and root exudate production (De-Ville et al., 2017; Bouzouidja et al., 2018; De-Ville et al., 2018; Yang & Davidson, 2021). Oxidation and "ageing" of biochar are also likely to alter hydrological properties (Wang et al., 2020). Future research should investigate the long-term hydrological performance of biochar-amended green roof substrates, accounting for time-dependent changes in substrate properties. In addition, future studies should evaluate the hydrological performance of granulated and unprocessed biochars under field conditions. Biochar application rate also plays a critical role in influencing the hydraulic properties of green roof substrates (Werdin et al., 2021). In this study, biochars were applied at a rate of 4.5% w/w (equivalent to ~25 t/ha), targeting optimal plant performance (Gale & Thomas, 2019). Future research should explore the optimal application rates that balance enhanced hydrological performance with improved vegetation growth and discharge water quality. Additional studies on alternative binding agents are also needed to optimize the properties of granulated biochar (Thomas, 2021), with the goal of improving hydrological performance and enhancing plant available water.

5. Conclusions

Our study shows that biochar granulation enhances the uniformity of surface and pore characteristics, resulting in more consistent effects on hydraulic properties across particle size ranges. In contrast, the BET specific surface area, total pore volume, and microporosity of unprocessed biochars increased with decreasing particle sizes. The addition of granulated biochar increased substrate field capacity, potentially enhancing stormwater retention on green roofs. However, a substantial portion of the retained water was tightly bound within biochar intrapores and thus not readily available to plants, though it should also be noted that the permanent wilting point metric has important limitations (e.g., Garg et al. (2020)). In contrast, the amendment of unprocessed biochars in the 0.5–1 mm and 2–2.8 mm size ranges enhanced plant available water, which is crucial for supporting vegetation performance on green roofs, particularly under prolonged drought conditions. Our results also show that the addition of fine unprocessed biochars reduced saturated hydraulic conductivity, indicating enhanced detention capacity through decreased infiltration rates and delayed peak flows. However, the use of fine biochar particles (e.g., < 1 mm) may increase the risks of human exposure to dust, erosion losses, and periodic waterlogging. Overall, granulated biochar and intermediate-sized unprocessed biochar may provide balanced stormwater retention and detention capacities, as well as enhanced plant available water on green roofs. Our study provides critical insights and key modeling parameters on the effects of biochar post-processing, especially granulation and particle size modification, on hydraulic properties and hydrological processes of green roof substrates. Granulated biochar, with demonstrated benefits for water quality improvement, enhanced plant performance, and

erosion control, holds strong potential for urban green infrastructure applications, thereby contributing to long-term urban sustainability.

Declarations

Competing interests

The authors declare no competing interests.

Acknowledgements

We thank Dr. Melanie Sifton, Dr. Maria Semeniuk, Dr. Murray Grabinsky, and Dr. Mohini Sain for their assistance with instrumentation and data collection, and Titan Clean Energy Projects Co., Gro-Bark Inc., and Bioroof Systems Inc. for providing experimental materials and relevant product information. This study was supported by grants from the Natural Sciences and Engineering Research Council of Canada (NSERC) Collaborative Research and Training Experience Program (CREATE) to J.D. and S.C.T, NSERC Discovery Grants Program to S.C.T, and Ontario Graduate Scholarship and NSERC Postdoctoral Fellowship to W.L.

Author contributions

Conceptualization: W.L., J.D. and S.C.T. Methodology: W.L., J.D. and S.C.T. Investigation: W.L. Formal analysis: W.L. Visualization: W.L. Writing – Original Draft: W.L. Funding acquisition: J.D. and S.C.T. Writing – Review & Editing: all authors.

References

Alghamdi, A. G., Alkhasha, A., & Ibrahim, H. M. (2020). Effect of biochar particle size on water retention and availability in a sandy loam soil. *J. Saudi Chem. Soc.*, *24*(12), 1042–1050. https://doi.org/10.1016/j.jscs.2020.11.003

Alim, M. A., Rahman, A., Tao, Z., Garner, B., Griffith, R., & Liebman, M. (2022). Green roof as an effective tool for sustainable urban development: An Australian perspective in relation to stormwater and building energy management. *J. Clean. Prod. 362*, 132561. https://doi.org/10.1016/j.jclepro.2022.132561

Bardestani, R., Patience, G. S., & Kaliaguine, S. (2019). Experimental methods in chemical engineering: Specific surface area and pore size distribution measurements—BET, BJH, and DFT. *Can. J. Chem. Eng.*, *97*(11), 2781–2791. https://doi.org/10.1002/cjce.23632

Benjamini, Y., & Hochberg, Y. (1995). Controlling the false discovery rate: A practical and powerful approach to multiple testing. *J. R. Stat. Soc. Ser. B Methodol.*, *57*(1), 289–300. https://doi.org/10.1111/j.2517-6161.1995.tb02031.x

Bouzouidja, R., Séré, G., Claverie, R., Ouvrard, S., Nuttens, L., & Lacroix, D. (2018). Green roof aging: Quantifying the impact of substrate evolution on hydraulic performances at the lab-scale. *J. Hydrol.*, *564*, 416–423. https://doi.org/10.1016/j.jhydrol.2018.07.032

Bowden-Green, B., & Briens, L. (2016). An investigation of drum granulation of biochar powder. *Powder Technol.*, *288*, 249–254. https://doi.org/10.1016/j.powtec.2015.10.046

Briens, L., & Bowden-Green, B. (2019). A comparison of drum granulation of biochars. *Powder Technol.*, *343*, 723–732. https://doi.org/10.1016/j.powtec.2018.11.077

Cao, C. T. N., Farrell, C., Kristiansen, P. E., & Rayner, J. P. (2014). Biochar makes green roof substrates lighter and improves water supply to plants. *Ecol. Eng.*, *71*, 368–374. https://doi.org/10.1016/j.ecoleng.2014.06.017

677 Cassel, D. K., & Nielsen, D. R. (1986). Field capacity and available water capacity. *Meth. Soil*
678 *Anal. Pt. 1*, *5*, 901–926.
679 Chen, Y., Zhou, H., Zhang, H., Du, G., & Zhou, J. (2015). Urban flood risk warning under rapid
680 urbanization. *Environ. Res.*, *139*, 3–10. https://doi.org/10.1016/j.envres.2015.02.028
681 Dai, L., Lu, Q., Zhou, H., Shen, F., Liu, Z., Zhu, W., & Huang, H. (2021). Tuning oxygenated
682 functional groups on biochar for water pollution control: A critical review. . *Hazard.*
683 *Mater.*, *420*, 126547. https://doi.org/10.1016/j.jhazmat.2021.126547
684 De-Ville, S., Menon, M., Jia, X., Reed, G., & Stovin, V. (2017). The impact of green roof ageing
685 on substrate characteristics and hydrological performance. *J. Hydrol.*, *547*, 332–344.
686 https://doi.org/10.1016/j.jhydrol.2017.02.006
687 De-Ville, S., Menon, M., & Stovin, V. (2018). Temporal variations in the potential hydrological
688 performance of extensive green roof systems. *J. Hydrol.*, *558*, 564–578.
689 https://doi.org/10.1016/j.jhydrol.2018.01.055
690 Donat, M. G., Lowry, A. L., Alexander, L. V., O'Gorman, P. A., & Maher, N. (2016). More
691 extreme precipitation in the world's dry and wet regions. *Nat. Clim. Change*, *6*(5), 508–
692 513. https://doi.org/10.1038/nclimate2941
693 Dos Santos Júnior, J. M., Fernandes, L. A., Colen, F., Frazão, L. A., & Pegoraro, R. F. (2025).
694 Biochar-Based Granular Fertilizers with Agro-Industrial Binders Enhance Enzymatic
695 Activity and Nutrient Cycling in Tropical Oxisols. *Agronomy*, *15*(9), 2230.
696 https://doi.org/10.3390/agronomy15092230
697 Edeh, I. G., & Mašek, O. (2021). The role of biochar particle size and hydrophobicity in
698 improving soil hydraulic properties. *Eur. J. Soil Sci.*, ejss.13138.
699 https://doi.org/10.1111/ejss.13138

Esmaeelnejad, L., Shorafa, M., Gorji, M., & Hosseini, S. mossa. (2017). Impacts of woody biochar particle size on porosity and hydraulic conductivity of biochar-soil mixtures: An incubation study. *Commun. Soil Sci. Plant Anal.*, *48*(14), 1710–1718. https://doi.org/10.1080/00103624.2017.1383414

Fahmi, A. H., Samsuri, A. W., Jol, H., & Singh, D. (2018). Physical modification of biochar to expose the inner pores and their functional groups to enhance lead adsorption. *RSC Adv.*, *8*(67), 38270–38280. https://doi.org/10.1039/C8RA06867D

Fan, M., Li, C., Shao, Y., Zhang, S., Gholizadeh, M., & Hu, X. (2022). Pyrolysis of cellulose: Correlation of hydrophilicity with evolution of functionality of biochar. *Sci. Total Environ.*, *825*, 153959. https://doi.org/10.1016/j.scitotenv.2022.153959

Gale, N. V., & Thomas, S. C. (2019). Dose-dependence of growth and ecophysiological responses of plants to biochar. *Sci. Total Environ.*, *658*, 1344–1354. https://doi.org/10.1016/j.scitotenv.2018.12.239

Gan, L., Garg, A., Wang, H., Mei, G., & Liu, J. (2021). Influence of biochar amendment on stormwater management in green roofs: Experiment with numerical investigation. *Acta Geophys.*, *69*(6), 2417–2426. https://doi.org/10.1007/s11600-021-00685-4

Gao, H., & Shao, M. (2015). Effects of temperature changes on soil hydraulic properties. *Soil Till. Res.*, *153*, 145–154. https://doi.org/10.1016/j.still.2015.05.003

Garg, A., Bordoloi, S., Ganesan, S. P., Sekharan, S., & Sahoo, L. (2020). A relook into plant wilting: Observational evidence based on unsaturated soil–plant-photosynthesis interaction. *Sci. Rep.*, *10*(1), 22064. https://doi.org/10.1038/s41598-020-78893-z

Haghverdi, A., Najarchi, M., Öztürk, H. S., & Durner, W. (2020). Studying unimodal, bimodal, PDI and bimodal-PDI variants of multiple soil water retention models: I. Direct model fit

723 using the extended evaporation and dewpoint methods. *Water*, *12*(3), 900.
724 https://doi.org/10.3390/w12030900
725 Haghverdi, A., Öztürk, H. S., & Durner, W. (2020). Studying unimodal, bimodal, PDI and
726 bimodal-PDI variants of multiple soil water retention models: II. Evaluation of
727 parametric pedotransfer functions against direct fits. *Water*, *12*(3), 896.
728 https://doi.org/10.3390/w12030896
729 Halim, M. A., Vantellingen, J., Gorgolewski, A. S., Rose, W. K., Drake, J. A. P., Margolis, L., &
730 Thomas, S. C. (2022). Greenhouse gases and green roofs: Carbon dioxide and methane
731 fluxes in relation to substrate characteristics. *Urban Ecosyst.*, *25*(2), 487–498.
732 https://doi.org/10.1007/s11252-021-01166-8
733 Hammond, M. J., Chen, A. S., Djordjević, S., Butler, D., & Mark, O. (2015). Urban flood impact
734 assessment: A state-of-the-art review. *Urban Water J.*, *12*(1), 14–29.
735 https://doi.org/10.1080/1573062X.2013.857421
736 Hill, J., Sleep, B., Drake, J., & Fryer, M. (2019). The effect of intraparticle porosity and
737 interparticle voids on the hydraulic properties of soilless media. *Vadose Zone J.*, *18*(1), 0.
738 https://doi.org/10.2136/vzj2018.09.0176
739 Hu, Q., Shao, J., Yang, H., Yao, D., Wang, X., & Chen, H. (2015). Effects of binders on the
740 properties of bio-char pellets. *Appl. Energy*, *157*, 508–516.
741 https://doi.org/10.1016/j.apenergy.2015.05.019
742 Huang, S., Garg, A., Mei, G., Huang, D., Chandra, R. B., & Sadasiv, S. G. (2020). Experimental
743 study on the hydrological performance of green roofs in the application of novel biochar.
744 *Hydrol. Process.*, 14.

745 Hussain, R., & Ravi, K. (2021). Investigating unsaturated hydraulic conductivity and water
746 retention characteristics of compacted biochar-amended soils for potential application in
747 bioengineered structures. *J. Hydrol.*, *603*, 127040.
748 https://doi.org/10.1016/j.jhydrol.2021.127040
749 Ibrahim, A., Usman, A. R. A., Al-Wabel, M. I., Nadeem, M., Ok, Y. S., & Al-Omran, A. (2017).
750 Effects of conocarpus biochar on hydraulic properties of calcareous sandy soil: Influence
751 of particle size and application depth. *Arch. Agron. Soil Sci.*, *63*(2), 185–197.
752 https://doi.org/10.1080/03650340.2016.1193785
753 Iden, S. C., & Durner, W. (2014). Comment on "Simple consistent models for water retention
754 and hydraulic conductivity in the complete moisture range" by A. Peters:
755 COMMENTARY. *Water Resour. Res.*, *50*(9), 7530–7534.
756 https://doi.org/10.1002/2014WR015937
757 Jaafar, N. M., Clode, P. L., & Abbott, L. K. (2015). Soil microbial responses to biochars varying
758 in particle size, surface and pore properties. *Pedosphere*, *25*(5), 770–780.
759 https://doi.org/10.1016/S1002-0160(15)30058-8
760 Kourtis, I. M., & Tsihrintzis, V. A. (2021). Adaptation of urban drainage networks to climate
761 change: A review. *Sci. Total Environ.*, *771*, 145431.
762 https://doi.org/10.1016/j.scitotenv.2021.145431
763 Lee, J., & Kwon, E. E. (2024). Biochar in green roofs. *J. Build. Eng.*, *89*, 109272.
764 https://doi.org/10.1016/j.jobe.2024.109272
765 Leng, L. (2021). An overview on engineering the surface area and porosity of biochar. *Sci. Total*
766 *Environ.*, 763, 144204. https://doi.org/10.1016/j.scitotenv.2020.144204

767 Li, Y., & Babcock, R. W. (2014). Green roof hydrologic performance and modeling: A review.
768 *Water Sci. Technol.*, *69*(4), 727–738. https://doi.org/10.2166/wst.2013.770
769 Liao, W., Drake, J., & Thomas, S. C. (2022a). Biochar granulation enhances plant performance
770 on a green roof substrate. *Sci. Total Environ.*, *813*, 152638.
771 https://doi.org/10.1016/j.scitotenv.2021.152638
772 Liao, W., Drake, J., & Thomas, S. C. (2022b). Biochar granulation, particle size, and vegetation
773 effects on leachate water quality from a green roof substrate. *J. Environ. Manage.*, *318*,
774 115506. https://doi.org/10.1016/j.jenvman.2022.115506
775 Liao, W., Halim, M. A., Kayes, I., Drake, J. A. P., & Thomas, S. C. (2023). Biochar Benefits
776 Green Infrastructure: Global Meta-Analysis and Synthesis. *Environ. Sci. Technol.*,
777 *57*(41), 15475–15486. https://doi.org/10.1021/acs.est.3c04185
778 Liao, W., Sifton, M. A., & Thomas, S. C. (2022c). Biochar granulation reduces substrate erosion
779 on green roofs. *Biochar*, *4*(1), 61. https://doi.org/10.1007/s42773-022-00186-7
780 Liao, W., & Thomas, S. C. (2019). Biochar particle size and post-pyrolysis mechanical
781 processing affect soil pH, water retention capacity, and plant performance. *Soil Syst.*,
782 *3*(1), 14. https://doi.org/10.3390/soilsystems3010014
783 Lu, S., & Zong, Y. (2018). Pore structure and environmental serves of biochars derived from
784 different feedstocks and pyrolysis conditions. *Environ. Sci. Pollut. Res.*, *25*(30), 30401–
785 30409. https://doi.org/10.1007/s11356-018-3018-7
786 Madsen, H., Lawrence, D., Lang, M., Martinkova, M., & Kjeldsen, T. R. (2014). Review of
787 trend analysis and climate change projections of extreme precipitation and floods in
788 Europe. *J. Hydrol.*, *519*, 3634–3650. https://doi.org/10.1016/j.jhydrol.2014.11.003

789 Nagase, A., & Dunnett, N. (2012). Amount of water runoff from different vegetation types on
790 extensive green roofs: Effects of plant species, diversity and plant structure. *Landsc.*
791 *Urban Plan.*, *104*(3–4), 356–363. https://doi.org/10.1016/j.landurbplan.2011.11.001
792 Oberndorfer, E., Lundholm, J., Bass, B., Coffman, R. R., Doshi, H., Dunnett, N., Gaffin, S.,
793 Köhler, M., Liu, K. K. Y., & Rowe, B. (2007). Green roofs as urban ecosystems:
794 Ecological structures, functions, and services. *BioScience*, *57*(10), 823–833.
795 https://doi.org/10.1641/B571005
796 Palermo, S. A., Turco, M., Principato, F., & Piro, P. (2019). Hydrological effectiveness of an
797 extensive green roof in Mediterranean climate. *Water*, *11*(7), 1378.
798 https://doi.org/10.3390/w11071378
799 Peng, Z., Smith, C., & Stovin, V. (2019). Internal fluctuations in green roof substrate moisture
800 content during storm events: Monitored data and model simulations. *J. Hydrol.*, *573*,
801 872–884. https://doi.org/10.1016/j.jhydrol.2019.04.008
802 Pertassek, T., A., P., & Wolfgang, D. (2015). *HYPROP-FIT Software User's Manual* (Version
803 V3.0) [Computer software]. UMS GmbH.
804 Peters, A. (2013). Simple consistent models for water retention and hydraulic conductivity in the
805 complete moisture range: Hydraulic Models for the Complete Moisture Range. *Water*
806 *Resour. Res.*, *49*(10), 6765–6780. https://doi.org/10.1002/wrcr.20548
807 Peters, A., & Durner, W. (2008). Simplified evaporation method for determining soil hydraulic
808 properties. *J. Hydrol.*, *356*(1–2), 147–162. https://doi.org/10.1016/j.jhydrol.2008.04.016
809 Petreje, M., Sněhota, M., Šípek, V., Hnátková, T., Punčochář, J., Buchtelík, S., Hardman, M., &
810 Trakal, L. (2025). Quantifying the benefits of incorporating biochar in green roof

substrates: Field study on the highrise rooftop in temperate climate setting. *Biochar*, *7*(1), 7. https://doi.org/10.1007/s42773-024-00409-z

R Core Team. (2024). *R: A language and environment for statistical computing* [Computer software]. R Foundation for Statistical Computing.

Rabbi, S. M. F., Minasny, B., McBratney, A. B., Young, I. M., & Salami, S. T. (2021). Greater, but not necessarily better: The influence of biochar on soil hydraulic properties. *Eur. J. Soil Sci.*, *72*(5), 2033–2048.

Razzaghi, F., Obour, P. B., & Arthur, E. (2020). Does biochar improve soil water retention? A systematic review and meta-analysis. *Geoderma*, *361*, 114055. https://doi.org/10.1016/j.geoderma.2019.114055

Rentschler, J. (2023). Global evidence of rapid urban growth in flood zones since 1985. *Nature*, *622*, 87–92. https://doi.org/10.1038/s41586-023-06468-9

Ritchie, H., & Roser, M. (2022, June 23). *Urbanization*. OurWorldInData.Org. https://ourworldindata.org/urbanization

Shi, W., Zhang, Y., Wei, Z., Weihermüller, L., Schaap, M. G., & Vereecken, H. (2026). Identifying and characterizing bimodal soil hydraulic properties through water retention curve analysis. *J. Hydrol.*, *666*, 134808. https://doi.org/10.1016/j.jhydrol.2025.134808

Sigmund, G., Hüffer, T., Hofmann, T., & Kah, M. (2017). Biochar total surface area and total pore volume determined by N2 and CO2 physisorption are strongly influenced by degassing temperature. *Sci. Total Environ.*, *580*, 770–775. https://doi.org/10.1016/j.scitotenv.2016.12.023

832 Stovin, V., Poë, S., De-Ville, S., & Berretta, C. (2015). The influence of substrate and
833 vegetation configuration on green roof hydrological performance. *Ecol. Eng.*, *85*, 159–
834 172. https://doi.org/10.1016/j.ecoleng.2015.09.076
835 Tan, K., & Wang, J. (2023). Substrate modified with biochar improves the hydrothermal
836 properties of green roofs. *Environ. Res.*, *216*, 114405.
837 https://doi.org/10.1016/j.envres.2022.114405
838 Tang, E., Liao, W., & Thomas, S. C. (2023). Optimizing Biochar Particle Size for Plant Growth
839 and Mitigation of Soil Salinization. *Agronomy*, *13*(5), 1394.
840 https://doi.org/10.3390/agronomy13051394
841 Thomas, S. C. (2021). Post-processing of biochars to enhance plant growth responses: A review
842 and meta-analysis. *Biochar*, *3*(4), 437–455. https://doi.org/10.1007/s42773-021-00115-0
843 Trifunovic, B., Gonzales, H. B., Ravi, S., Sharratt, B. S., & Mohanty, S. K. (2018). Dynamic
844 effects of biochar concentration and particle size on hydraulic properties of sand. *Land*
845 *Degrad. Dev.*, *29*(4), 884–893. https://doi.org/10.1002/ldr.2906
846 Van Genuchten, M. Th. (1980). A closed-form equation for predicting the hydraulic conductivity
847 of unsaturated soils. *Soil Sci. Soc. Am. J., 44*(5), 892–898.
848 https://doi.org/10.2136/sssaj1980.03615995004400050002x
849 Wang, D., Li, C., Parikh, S. J., & Scow, K. M. (2019). Impact of biochar on water retention of
850 two agricultural soils – A multi-scale analysis. *Geoderma*, *340*, 185–191.
851 https://doi.org/10.1016/j.geoderma.2019.01.012
852 Wang, L., O'Connor, D., Rinklebe, J., Ok, Y. S., Tsang, D. C. W., Shen, Z., & Hou, D. (2020).
853 Biochar aging: Mechanisms, physicochemical changes, assessment, and implications for
854 field applications. *Environ. Sci. Technol.*

Werdin, J., Conn, R., Fletcher, T. D., Rayner, J. P., Williams, N. S. G., & Farrell, C. (2021). Biochar particle size and amendment rate are more important for water retention and weight of green roof substrates than differences in feedstock type. *Ecol. Eng.*, *171*, 106391. https://doi.org/10.1016/j.ecoleng.2021.106391

Wolf, D., & Lundholm, J. T. (2008). Water uptake in green roof microcosms: Effects of plant species and water availability. *Ecol. Eng.*, *33*(2), 179–186. https://doi.org/10.1016/j.ecoleng.2008.02.008

Yang, Y., & Davidson, C. I. (2021). Green roof aging effect on physical properties and hydrologic performance. *J. Sustain. Water Built Environ., 7*(3), 04021007. https://doi.org/10.1061/JSWBAY.0000949

Yazdanfar, Z., & Sharma, A. (2015). Urban drainage system planning and design – challenges with climate change and urbanization: A review. *Water Sci. Technol.*, *72*(2), 165–179. https://doi.org/10.2166/wst.2015.207

Zanutel, M., Garré, S., Sanglier, P., & Bielders, C. (2024). Biochar modifies soil physical properties mostly through changes in soil structure rather than through its internal porosity. *Vadose Zone J.*, *23*(1), e20301. https://doi.org/10.1002/vzj2.20301

Zhang, J., Amonette, J. E., & Flury, M. (2021). Effect of biochar and biochar particle size on plant-available water of sand, silt loam, and clay soil. *Soil Till. Res.*, *212*, 104992. https://doi.org/10.1016/j.still.2021.104992

Zhao, Y., Rahardjo, H., Satyanaga, A., Zhai, Q., & He, J. (2023). A general best-fitting equation for the multimodal soil–water characteristic curve. *Geotech. Geol. Eng.*, *41*(5), 3239–3252. https://doi.org/10.1007/s10706-023-02447-z

877 Zheng, X. (2021). Green roofs for stormwater runoff retention: A global quantitative synthesis of
878 the performance. *Resour. Conserv. Recy.*, 170, 105577.
879 https://doi.org/10.1016/j.resconrec.2021.105577
880
881

Tables

Table 1. Two-way ANOVA outputs for the surface area and pore characteristics of factorial treatment (granulated and unprocessed biochars in 1-2 mm, 2-2.8 mm, and 2.8-4 mm particle size ranges). PM and PS indicate biochar processing method (granulated vs. unprocessed biochars) and particle size, respectively. Asterisks indicate significance of two-way ANOVA: (*), $P < 0.1$; *, $P < 0.05$; **, $P < 0.01$; ***, $P < 0.001$.

Source of variation	df	Sum of Squares	Mean Square	F	*P*
BET specific surface area					
PM	1	15496	15496	26.30	**0.002** **
PS	2	8123	4061	6.89	**0.028** *
PM × PS	2	16933	8467	14.37	**0.005** **
Error	6	3535	589		
Total pore volume					
PM	1	0.0043	0.0043	15.92	**0.007** **
PS	2	0.0022	0.0011	3.94	0.081 (*)
PM × PS	2	0.0072	0.0036	13.27	**0.006** **
Error	6	0.0016	0.0003		
Average pore diameter					
PM	1	8.0803	8.0803	32.35	**0.001** **
PS	2	2.2648	1.1324	4.53	0.063 (*)
PM × PS	2	7.4281	3.7141	14.87	**0.005** **
Error	6	1.4987	0.2498		
Micropore volume					
PM	1	0.00593	0.00593	33.40	**0.001** **
PS	2	0.00287	0.00144	8.09	**0.020** *
PM × PS	2	0.00607	0.00303	17.07	**0.003** **
Error	6	0.00107	0.00018		
Mesopore volume					

PM	1	0.00012	0.00012	3.52	0.110
PS	2	0.00008	0.00004	1.18	0.370
PM × PS	2	0.00005	0.00003	0.75	0.513
Error	6	0.00021	0.00004		
Percentage of micropore					
PM	1	1987.8	1987.8	191.25	**< 0.001** ***
PS	2	409.9	205.0	19.72	**0.002** **
PM × PS	2	496.6	248.3	23.89	**0.001** **
Error	6	62.4	10.4		
Percentage of mesopore					
PM	1	1987.8	1987.8	191.25	**< 0.001** ***
PS	2	409.9	205.0	19.72	**0.002** **
PM × PS	2	496.6	248.3	23.89	**0.001** **
Error	6	62.4	10.4		

889

890 **Table 2.** One-way ANOVA outputs for the biochar particle size effects on surface area and pore characteristics for unprocessed and
891 granulated biochars. Asterisks indicate significance of two-way ANOVA: (*), $P < 0.1$; *, $P < 0.05$; **, $P < 0.01$; ***, $P < 0.001$.
892

Source of variation	**Biochar particle size**			
	Unprocessed biochar		**Granulated biochar**	
	F(4, 5)	***P***	**F(3, 4)**	***P***
BET specific surface area	36.703	**< 0.001** ***	1.104	0.4451
Total pore volume	42.785	**< 0.001** ***	1.074	0.4545
Average pore diameter	14.476	**0.006** **	2.448	0.2036
Micropore volume	36.963	**< 0.001** ***	1.096	0.4476
Mesopore volume	0.873	0.5394	1.044	0.4643
Percentage of micropore	21.575	**0.002** **	2.055	0.2489
Percentage of mesopore	21.575	**0.002** **	2.055	0.2489

893

Table 3. Two-way ANOVA outputs for the hydraulic properties of factorial treatment (granulated and unprocessed biochars in 1-2 mm, 2-2.8 mm, and 2.8-4 mm particle size ranges). PM and PS indicate biochar processing method (granulated vs. unprocessed biochars) and particle size, respectively. Asterisks indicate significance of two-way ANOVA: (*), $P < 0.1$; *, $P < 0.05$; **, $P < 0.01$; ***, $P < 0.001$.

Source of variation	df	Sum of Squares	Mean Square	F	*P*
Field capacity					
PM	1	14.04	14.04	53.69	**<0.001** ***
PS	2	4.35	2.17	8.31	**0.019** *
PM × PS	2	1.26	0.63	2.42	0.170
Error	6	1.57	0.26		
Permanent wilting point					
PM	1	16.52	16.52	7.98	**0.030** *
PS	2	9.18	4.59	2.22	0.190
PM × PS	2	2.44	1.22	0.59	0.584
Error	6	12.43	2.07		
Plant available water					
PM	1	0.10	0.10	0.08	0.786
PS	2	25.45	12.72	10.13	**0.012** *
PM × PS	2	1.13	0.57	0.45	0.657
Error	6	7.53	1.26		
Saturated hydraulic conductivity					
PM	1	558977	558977	0.11	0.751
PS	2	152832303	76416151	14.46	**< 0.001** ***
PM × PS	2	133634277	66817138	12.64	**< 0.01** **
Error	12	63422172	5285181		